

# Fully Passive Robotic Finger for Human-Inspired Adaptive Grasping in Environmental Constraints

Dukchan Yoon<sup>✉</sup>, Member, IEEE, and Keehoon Kim<sup>✉</sup>, Member, IEEE

**Abstract**—This article presents an adaptive finger mechanism for grasping objects in an environmental constraint. The proposed finger is designed such that it can be easily installed to a parallel gripper, and hence, operated using a single linear actuation system. The parallel gripper equipped with the proposed finger mechanism features capabilities of self-adaptation to various object shapes and interaction with environmental constraints. Besides, based on the interaction capability with environments, robotic grasping strategies inspired by human grasping approaches such as adaptive pinching and scooping are achieved. In particular, two types of scooping approaches corresponding to the symmetric and asymmetric configurations of the gripper are introduced. In this regard, Hart's linkage mechanism coupled with a parallelogram is applied to the proposed finger mechanism to synthesize the vertical translation for finger compliance as well as the unique transition motion between the pinching and scooping poses of the fingertip. These two degrees of freedom are entirely passive and can adapt to unknown objects or environmental constraints. The operating principle, limitations, and design guidelines for the proposed finger mechanism are analyzed through kinematics and statics. The fully prototyped two-finger gripper is evaluated through several demonstration scenarios to verify human-inspired grasping with objects of arbitrary shapes in environmental constraints.

**Index Terms**—Finger compliance, human-inspired grasping, robot–environment interaction, straight-line mechanism.

## I. INTRODUCTION

**G**RASPING is an essential function of the human hand. As shown at the top of Fig. 1, the human hand uses different approaches to grasp an object. Its finger interacts with an envi-

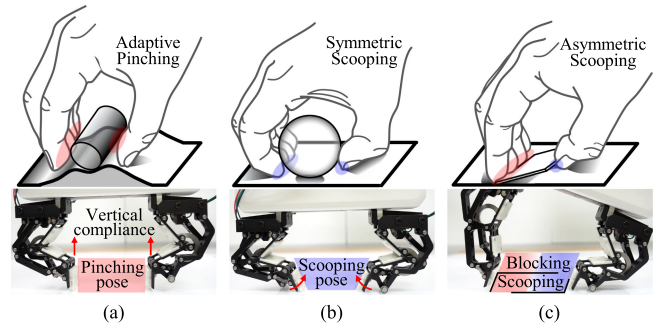


**Fig. 1.** Three typical approaches of human grasping and human-inspired grasping of parallel gripper equipped with proposed finger mechanism. (a) Adaptive pinching grasp in environmental constraint. (b) Symmetric scooping for stable enveloping. (c) Asymmetric scooping for stable pinching grasp.

ronmental constraint to reach the object for successful grasping as sliding on an uneven constraint or surface [see Fig. 1(a)], flexing fingertips by the constraint [see Fig. 1(b)], and supporting the object on the constraint [see Fig. 1(c)] according to the size, shape, and state of the object. This article presents a fully passive self-adaptive finger mechanism that enables robotic grasping strategies inspired by those human grasping approaches to grasp diverse objects, interacting with an environmental constraint. In recent years, many research groups have developed robotic hands by designing an underactuated mechanism for mechanical compliance. The underactuated mechanism is defined as the mechanical system using the number of actuators less than the motion degrees of freedom (DOFs) [1]. Its mechanical compliance can be achieved by installing the number of elastic elements such as springs greater than or equal to the remaining DOFs. Thereby, this mechanism can be passively controlled by means of physical contact with constraints. These efforts have primarily focused on implementing passive intelligence such as self-adaptation to various object shapes, interaction with environmental constraints, and object manipulation for a stable grasping position.

The mechanical compliance of the underactuated mechanism enables the robotic finger to automatically envelop object shapes without a complex control algorithm. Several robotic fingers capable of self-adaptive grasping have been proposed. Laliberté *et al.* [1] developed a three-fingered gripper to manage diverse objects and analyze ejection with respect to a grasping equilibrium. Hong *et al.* [2] developed an underactuated hand exoskeleton for grasping that can mimic the natural flexion of the human index finger and envelope objects, which is similar

Manuscript received September 9, 2021; revised December 13, 2021; accepted January 18, 2022. Recommended by Technical Editor F. Auat Cheein and Senior Editor W. J. C. Zhang. This work was supported in part by the Korea Advanced Research Program through the National Research Foundation of Korea (NRF) funded by Ministry of Science and ICT under Grant 020M3H8A1114905, and in part by the Alchemist under Project (20012378), Development of Meta Soft Organ Module Manufacturing Technology without Immunity Rejection and Module Assembly Robot System funded by the Ministry of Trade, Industry and Energy (MOTIE, Korea). (*Corresponding author: Keehoon Kim*)

The authors are with the Department of Mechanical Engineering, Pohang University of Science and Technology (POSTECH), Pohang 37673, South Korea (e-mail: dcyon@postech.ac.kr; khk@postech.ac.kr).

This article has supplementary material provided by the authors and color versions of one or more figures available at <https://doi.org/10.1109/TMECH.2022.3145490>.

Digital Object Identifier 10.1109/TMECH.2022.3145490

to the study presented in [3]. More recently, Chang *et al.* [4] developed a prosthetic hand to firmly grasp objects in a dynamic situation, embodying human-like carpometacarpal joints in both the fourth and fifth robotic fingers, as inspired by the concavity of the human palm. Other robotic fingers for self-adaptive grasping were reviewed in [5].

Despite significant contributions to research pertaining to self-adaptive grasping recently, unexpected interactions with an environmental constraint renders it challenging for robotic hands to grasp objects. In many robotic grasping demonstrations, an object's posture is typically set to be grasped without contact with the environment. By contrast, the human fingers naturally adapt to environmental constraints as they slide on the cluttered surface of the environment to grasp small objects on the surface. Moreover, a grasping approach such as the pinching grasp or enveloping grasp is instinctively determined based on the size and shape of objects, where appropriate finger poses are adopted to achieve stable grasping. However, it is difficult for most underactuated hands composed of rigid bodies to perform human-like grasping in an environmental constraint because their mechanical compliance is often ineffective depending on the contact configuration of the environmental constraint. To adapt to an environment, soft mechanisms can be considered for robotic hand design. Soft robots make use of the softness of their body materials, as defined in [6], and their material properties enables robots to interact with environments without any damage. For instance, the RBO hands [7]–[9] demonstrate robust adaptability to the environment owing to their inherent softness. Additionally, Eppner *et al.* [9] reported that exploiting the environment rather than avoiding it results in robust and versatile grasping performance similar to that of human grasping. They argued that “*A competent grasper must exploit constraints present in the environment by employing physical contact so as to counteract uncertainty in state variables most relevant to grasp success.*” Furthermore, the Pisa/IIT SoftHand proposed in [10] demonstrated a self-adaptive grasping capability in a highly cluttered underwater environment [11]. In rigid mechanisms regarded as relatively low in compliance but preferred for applications requiring high stiffness, precision, and repeatability in grasping, a method to design a linkage-driven finger mechanism to achieve adaptability to more complex environments has been proposed through the analysis of a fingertip force vector in our previous article [12]. Although various experimental evaluations supported the robust environmental adaptability in our related work, it is still limited to only the simple pinching grasp or enveloping grasp without object manipulation such as flipping or scooping prior to grasping such that the object remains in a stable position.

To achieve stable grasping, a robotic hand should manipulate the object with the fingertips to maintain an appropriate hand posture while allowing adaptation to the environment during grasping. For example, when a human hand grasps thin objects with relatively large widths, such as a coin or a plastic card lying on a flat surface, the orientation of the object is manipulated by the fingertips with the support of the surface to secure a sufficient contact area of the object without establishing contact with the edges. Although many practical solutions exist that use soft mechanisms and suction caps [13]–[15] or additional

mechanical components on the fingertip, e.g., the crawler mechanism [16] and the sheet-wrapped belt [17], these approaches are outside the scope of our study. We believe that a human-inspired grasping strategy can be achieved using a rigid underactuated finger mechanism with minimal numbers of actuators and sensors. Human-inspired grasping motions have been implemented using underactuated robotic fingers. Odhner *et al.* [18]–[20] presented a human-inspired flipping motion of thin objects such as coins and keys. In this regard, whereas one fingertip pins one side of the coin against the surface to pivot about the tip, an opposing fingertip lifts and rotates on the other side of the coin. The coin is then flipped into the pinching grasp between the fingertips. Similarly, Jiang *et al.* [21] presented a flex-and-flip method for manipulating a deformable thin object such as a paper to pinch it. Babin and Gosselin [22], [23] proposed the scooping motion of a thumb mechanism. In this regard, whereas the fingertip shields one side of the thin object, the opposed fingertip slips under the object to be stably shifted into the pinching grasp. To penetrate the gap between the object and surface, the tip of the fingertip should be sharp. Nishimura [24] applied scooping to lift an object for an enveloping grasp. Hence, the scooping method is effective for stably manipulating thin objects, as proposed in many previous studies [25], [26].

In our study, we attempted to implement an underactuated robotic gripper that fulfills the following requirements:

- 1) Self-adaptation to various object shapes.
- 2) Self-adaptation to environmental constraints.
- 3) Fully passive finger mechanism operated by only a single linear actuation.
- 4) Human-inspired grasping motions, including the adaptive pinching grasp to pinch small objects in environmental constraints [see Fig. 1(a)], symmetric scooping to envelop large objects [see Fig. 1(b)], and asymmetric scooping to pinch thin objects with a large width [see Fig. 1(c)].

We conclude that, whereas the literature offers several valuable insights, a prototype that fulfills these requirements is yet to be developed. Hence, the following aspects were considered for two-DOF fingertip movements:

- 1) The vertical translation for the pinching pose to maintain finger compliance.
- 2) The orientation for the scooping pose, as shown at the bottom of Fig. 1(a) and (b), respectively.

Hence, the proposed prototype combines both Hart's linkage [28] and the parallelogram linkage. Furthermore, the proposed finger mechanism is designed to be attached easily to commercialized parallel grippers that use a single linear actuation system.

The rest of this article is organized as follows: In Section II, the advantage of finger compliance with a vertical path on a parallel gripper is highlighted based on investigations of possible finger movements for different paths. The geometric design of the proposed finger and its operating principle are described in Section III. Kinematics and statics analyses to determine the performance and limitations of the proposed prototype are presented in Section IV. The evaluation of the proposed prototype based on experiments and demonstrations to verify its practical feasibility and effectiveness is presented in Section V. Finally, Section VI concludes this article.

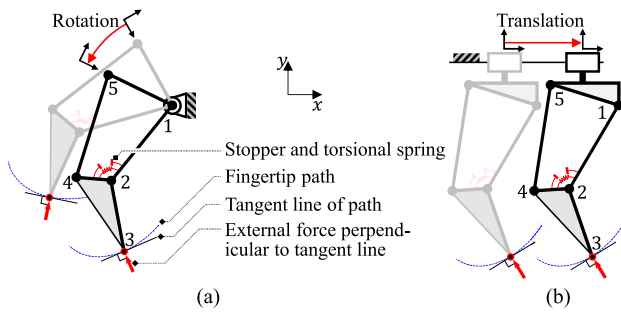


**Fig. 2.** Exemplary finger mechanism composed of four-bar linkage and its configuration to describe the finger compliance according to types of actuators. (a) Rotary actuation. (b) Linear actuation.

## II. FINGERTIP PATH FOR 1-DOF FINGER COMPLIANCE

Although an underactuated finger mechanism is mechanically compliant due to passive elements such as springs, the effectiveness of the compliance depends on the configurations of the underactuated finger and the environment because of limited DOFs. In this section, we present the design requirements of the finger mechanism to have robustness defined in [27] enabling qualitative interactions with prescribed environmental constraints for maintaining its grasping function against these contact disturbances.

### A. Linear Actuation for Consistent Finger Compliance

An actuating type plays a role to determine the configuration of a robotic finger. To show the compliance capability according to the actuating types, we provide an example of an underactuated finger based on a four-bar linkage, as illustrated in Fig. 2. This finger involves two-DOF driven by an actuation and spring. When the input link  $l_{15}$  as an actuation component is locked, the finger then exhibits a passive one-DOF with the spring. If an external force is applied to the fingertip, the finger will move with the deformation of the spring. At the same time, its fingertip traces its own unique path, as predefined by the lengths of the four links, with respect to the coordinate system attached to the link  $l_{15}$ . However, if the direction of the external force is perpendicular to the tangent line of the path at the position where the fingertip is, then the finger withstands the force structurally, which results in compliance loss. It is noteworthy that rotary actuation changes the configuration of the finger with respect to the global coordinates [see Fig. 2(a)]. It implies that the finger compliance differs depending on finger orientations for the same direction of the external force. By contrast, a linear actuation results in consistent compliance regardless of the finger position translated [see Fig. 2(b)]. Therefore, linear actuation is more beneficial to interacting with static and prescribed environmental constraints once the fingertip path is defined well.

Furthermore, linear actuation is widely used in lots of classical parallel-jaw grippers, which are commercially available for industrial manufacturing. These usually allow the replacement of types of jaws for various manufacturing tasks. If a proposed finger prototype is developed without including an actuation system, then it is expected to be easily attached to such parallel grippers. In recent years, such design philosophy has been

presented by Birglen [29], [30], who focused on enhancing the versatility and safety of commercialized grippers through replacing of the jaws with his finger mechanisms. Inspired by his studies, we are to design the proposed finger mechanism as the prototype with a mechanical adaptor that connects to the classical parallel grippers.

### B. Possible Movements of Fingers Based on Fingertip Paths

Design parameters of a mechanical system can define the fingertip path of a robotic finger to couple relative motions between phalanges (e.g., the lengths of links for the four-bar linkage shown in Fig. 2). Depending on defining a fingertip path, there can be lots of possible movements of two-phalanx finger. Inter alia, we introduce the possible movements interacting with a flat surface, based on two typical fingertip paths as illustrated in Fig. 3. It is noteworthy that no actuation component exists in this finger mechanism, except for the linear actuation of the gripper base. Instead, a spring and stopper were installed in the middle joint of the finger.

Let us consider that the fingertip path points in the right diagonal direction for the left finger such that the parallel gripper points to the inside of its grasping area in both of its paths [see Fig. 3(a)]. Subsequently, a manipulator (or a robot arm) attempts to fetch a fragile object on a flat surface. When approaching the object overhead, if the manipulator pushes down the surface with the gripper, then the fingers are flexed by the support of the surface, causing spring deformation. At that time, the fingertips passively approach each other along their paths, thereby squeezing the object. To ensure that the object is not damaged by squeezing, the opening speed of the linear actuator must be higher than the closing speed of the fingertips, thereby compensating for the fingertip position. Despite the successful compensation, the gripper can in fact overlook the object when the manipulator lifts the gripper because the spring energy causes the fingertips to open toward their initial positions as the whole fingers depart from the contact surface. Therefore, the kinematic relationship between the pushing or shifting speed of the manipulator and the opening or closing speed of the linear actuation should be considered comprehensively.

Let us consider another movement of the parallel gripper where both paths pointed toward the outside of the grasping area [see Fig. 3(b)]. When the gripper pushed the surface, the fingertips were passively opened. Hence, the gripper pinched the object, and the linear actuator should close until the fingertips were in contact with it. However, whether they can perform pinching successfully depends on the stroke range of the linear actuator or the object width. If the closing motion of the actuator reaches the end of the stroke range before the fingertips establish contact with the object, the gripper will fail to pinch. Furthermore, even if the fingertips perform pinching successfully, it is uncertain whether the gripper grasps the object continuously because the actuator cannot exert an appropriate pinching force at the end of the stroke. Only the spring effect governs the pinching force. Therefore, the gripper cannot grasp an object with a width smaller than the opening distance between the fingertips.

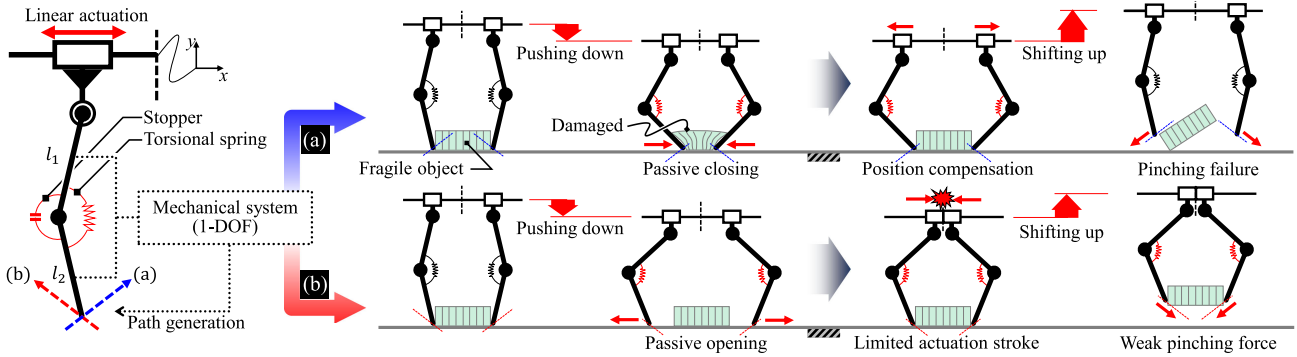


Fig. 3. Possible movements of two-phalanx fingers based on fingertip paths. (a) Right diagonal path. (b) Left diagonal path.

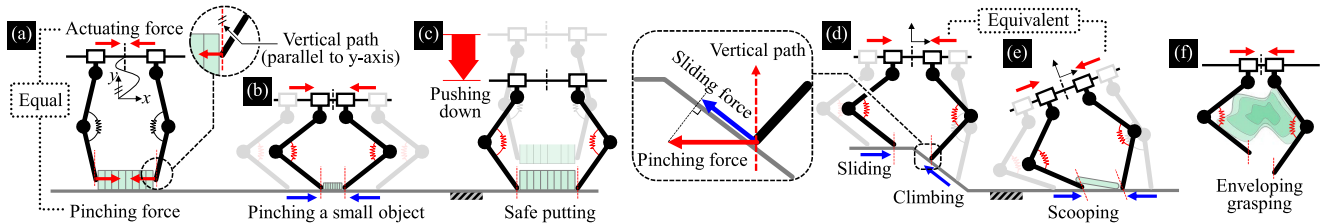


Fig. 4. Feasible movements of two-phalanx fingers with vertical path. (a) Pinching force equal to actuation due to horizontal constraint of fingertips. (b) Pinching a small object by support of surface. (c) Safely placing the object. (d) Sliding on surface. (e) Climbing on a thin object. (f) Enveloping grasping.

### C. Advantages of Vertical Fingertip Path on Parallel Gripper

In this article, we propose that finger compliance along a vertical fingertip path perpendicular to the gripper base (or parallel to the  $y$ -axis) is more advantageous to the interaction of the parallel gripper. The feasible performance of the gripper whose fingertips have the vertical path in the compliant direction is illustrated in Fig. 4. In other words, both fingertips are horizontally constrained for all finger configurations. Hence, the pinching force is the same as the linear actuation force when the gripper pinches the objects similarly as existing rigid jaws [see Fig. 4(a)]. Owing to the vertical compliance, the fingertips were stationary on the contact surface, whereas the manipulator pushed the gripper down. Therefore, the gripper can pinch small and thin objects before the actuation reaches the end of the stroke as well as safely place them on the surface without damage [see Fig. 4(b) and (c)], respectively. Moreover, the gripper can adapt to various environments by sliding on (or climbing) surfaces slanted at an acute angle, provided that a sufficient sliding force is generated at the fingertip [see Fig. 4(d)]. Similarly, the gripper can scoop a flat object via the sliding motion [see Fig. 4(e)]. In the case of grasping relatively large objects, the gripper can envelop their complex shapes using different configurations on each finger [see Fig. 4(f)].

## III. MECHANISM DESIGN

To order to implement the aforementioned vertical compliance of the finger mechanism, we introduce a straight-line mechanism, referred to as Hart's linkage, as proposed in [28]. This mechanism is in the form of an isosceles triangle with a

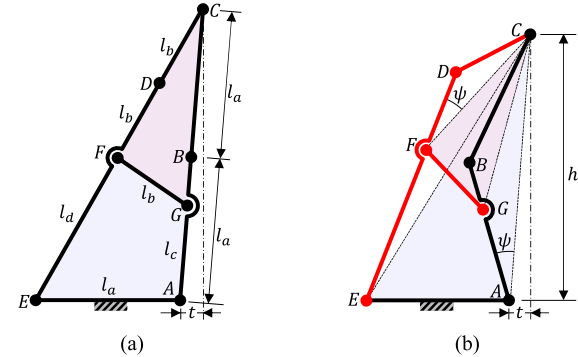


Fig. 5. Design parameters for generating vertical fingertip path of Hart's linkage with obtuse triangular form. (a) Fully stretched posture. (b) Slightly flexed posture.

single crosslink connecting the front and back—it is an A-shaped six-bar linkage. Its form resembles that of the finger mechanisms proposed in [29] and [30], unlike its kinematic definitions such as the DOF and fingertip path. To adapt to a finger mechanism, its design parameters were adjusted, thereby facilitating the opposition of the fingers, which exhibits an obtuse scalene triangular form.

### A. Fingertip Translation: Design of Offset Hart's Linkage for Vertical Compliance

A schematic diagram of Hart's linkage with an obtuse scalene triangular form is described in Fig. 5(a). We define the link parameters as follows:  $l_{AB}$ ,  $l_{BC}$ , and  $l_{AE}$  denote the first phalanx, second phalanx, and base link, respectively;  $l_{CD}$ ,  $l_{DE}$ , and  $l_{FG}$

denote the transmission links that enable tip  $C$  to trace the exact vertical path perpendicular to the base with an offset distance  $t$ . Especially,  $l_{AB}$  and  $l_{DE}$  were constructed as ternary links to bridge  $l_{FG}$  between them. Based on [28], these link parameters were used to generate the beginning of a vertical path using a similarity condition for triangles, as follows:  $\triangle CFG \sim \triangle CAE$  with angle  $\angle CAB = \angle CFD = \psi$ , as shown in Fig. 5(b), satisfying

$$\begin{aligned} l_{CG}/l_{FG} &= l_{CE}/l_{AE} \\ l_{BC}/l_{BG} &= l_{DE}/l_{CD} \\ l_{FG}/l_{AE} &= l_{BC}/l_{DE}. \end{aligned} \quad (1)$$

We set  $l_{AB} = l_{BC} = l_{AE} \triangleq l_a$ ,  $l_{CD} = l_{DF} = l_{FG} \triangleq l_b$ ,  $l_{AG} \triangleq l_c$ , and  $l_{FE} \triangleq l_d$  to simplify the design parameters, as shown in Fig. 5(a). Therefore, (1) can be expressed as follows:

$$l_{CG}/l_b = l_{CE}/l_a \quad (2)$$

$$l_a/(l_a - l_c) = (l_b + l_d)/l_b \quad (3)$$

$$l_b/l_a = l_a/(l_b + l_d) \quad (4)$$

where  $l_{CG}$  in (2) can be expressed using the law of cosine in  $\triangle CBG$  as

$$l_{CG}^2 = l_a^2 + (l_a - l_c)^2 + 2l_a(l_a - l_c) \cos 2\psi. \quad (5)$$

After squaring  $l_{CG} = l_{CE}l_b/l_a$  in (2) and substituting it into (5), we obtain

$$l_b^2 = l_{CE}^{-2}l_a^2l_c^2 - 4l_{CE}^{-2}l_a^3l_c \cos^2 \psi + 4l_{CE}^{-2}l_a^4 \cos^2 \psi \quad (6)$$

where  $l_b^2$  is also represented in terms of  $l_a$  and  $l_c$  by combining (3) and (4) as follows:

$$l_b^2 = l_a(l_a - l_c). \quad (7)$$

Subtracting (7) from (6), and then, arranging it, we can obtain the following quadratic equation in terms of  $l_c$ :

$$\epsilon_1 l_c^2 + \epsilon_2 l_c + \epsilon_3 = 0 \quad (8)$$

where  $\epsilon_1 = l_a^2 l_{EC}^{-2}$ ,  $\epsilon_2 = l_a(1 - 4\epsilon_1 \cos^2 \psi)$ , and  $\epsilon_3 = -l_a l_c$ .

Here, the  $l_a$  of each  $\epsilon_i$ , for  $i = 1, 2, 3$ , can be predetermined as the length of the phalanges and the width of the base. Subsequently, the angle  $\psi$  is known when the height  $h$  and offset  $t$ , which constitute the position coordinates of tip  $C$ , are assigned arbitrarily. At that time,  $l_{CE}$  and  $l_{AC}$  are obtained using the assigned values of  $\psi$  and  $l_a$  as well. Now,  $\epsilon_i$ , for  $i = 1, 2, 3$ , are constant coefficients.  $l_c$  can be solved using (8). Subsequently, both  $l_d$  and  $l_b$  can be solved simultaneously using (3) and (4). The designed links allow tip  $C$  to trace the exact vertical path with offset  $t$ .

It is clear that the fully stretched finger, as illustrated in Fig. 5(a), does not allow compliance when an external force is exerted on the tip  $C$  in any direction because of the instantaneous center of rotation of the four-bar linkage  $AGFE$  coincident with the tip  $C$ . Hence, an initial posture of the phalanges must be set such that the finger immediately absorbs the external force. Let the length of the phalanges be predetermined as  $l_a = 40$  mm. The height and offset were predetermined as  $h = 78$  mm and  $t = 10$  mm, respectively, which correspond to  $\psi = 10.59^\circ$ . For

**TABLE I**  
DESIGN RESULTS OF DIMENSIONAL PARAMETERS OF HART'S LINKAGE

| $t$   | $h(\psi)$              | Predetermined parameters |         |         | Designed parameters |  |  |
|-------|------------------------|--------------------------|---------|---------|---------------------|--|--|
|       |                        | $l_a$                    | $l_b$   | $l_c$   | $l_d$               |  |  |
| 10 mm | 78 mm ( $10.6^\circ$ ) | 40 mm                    | 22.4 mm | 27.5 mm | 49 mm               |  |  |

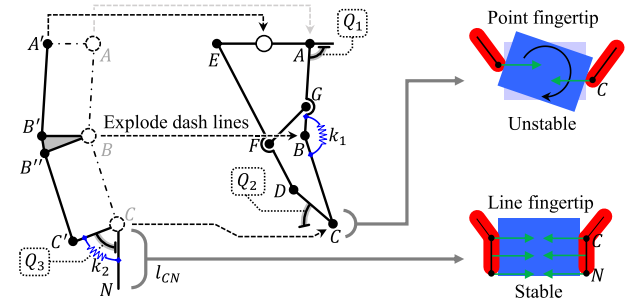


Fig. 6. Combination of offset Hart's linkage and parallelogram linkage with common joints,  $A$ ,  $B$ , and  $C$ , for pinching stability.

the specified  $l_a$ ,  $h$ , and  $t$ , all the designed parameters are listed in Table I. Additionally, as illustrated in Fig. 6, a spring  $k_1$  was installed in joint  $B$  to implement the finger compliance, and a stopper  $Q_1$  was structured into joint  $A$  as  $Q_1 = 93.28^\circ$  (corresponding to  $\psi = 10.59^\circ$ ) to prevent the full stretch of the finger.

### B. Fingertip Orientation: Design of Parallelogram Linkage for Scooping Pose

Thus far, we have discussed the movements of the two-phalanx finger. If a pair of Hart's linkages attempts to pinch an object by themselves, then the two-point contact of their tips will render the object unstable during grasping. A parallelogram linkage is widely used to develop a more stable pinching grasp because it enables a parallel line contact with the object, as shown in Fig. 6. This can be easily achieved by combining the parallelogram and Hart's linkage through shearing the phalanges with common joints  $A$ ,  $B$ , and  $C$ . If the link  $l_{CNC'}$  is considered as a single body (it will be separated into two segments subsequently), then its movement has a vertical translation with a constant orientation.

In this article, we developed a scooping pose for the fingertip. Scooping is a grasping strategy to guide an object that cannot be directly grasped inward toward the grasping area of the gripper for pinching or enveloping grasps. Hence, the fingertip should be tilted intentionally with an attack angle to slide under the object, thereby allowing contact with the surface. To implement the scooping pose of the proposed finger mechanism,  $l_{CNC'}$  was separated into segments  $l_{CN}$  and  $l_{CC'}$  as illustrated in Fig. 6. Meanwhile,  $l_{CN}$  was vertically supported by another stopper  $Q_3$  of  $l_{CC'}$  and the other spring  $k_2$ . Hereinafter,  $l_{CN}$  is referred to as the fingertip. The angle of  $Q_3$  was designed as  $Q_3 = 68^\circ$  (considering the intermediate angle  $\angle B'BB'' = 22^\circ$ ) such that the opposite fingertips were parallel. To trigger a transition to the scooping pose, the proposed finger exploits the other stopper  $Q_2$  of  $l_{CD}$ . As shown in Fig. 7, the fingertip performs the transition from the pinching pose to the scooping pose. While pushing the

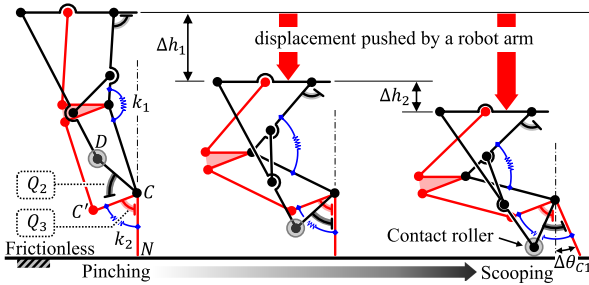


Fig. 7. Fingertip transition from pinching to scooping poses using stoppers.

TABLE II  
DIMENSIONS OF PARALLELOGRAM LINKAGE AND STOPPERS

| $l_{ii'}$   $i=A,B,C$ | $l_{A'B'}(l_{B''C'})$ | $l_{CN}$ | $\angle B'B B''$ | $Q_1$ | $Q_2$ | $Q_3$ |
|-----------------------|-----------------------|----------|------------------|-------|-------|-------|
| 20 mm                 | 40 mm                 | 27 mm    | 22°              | 93.3° | 47.7° | 68°   |

finger down,  $Q_3$  maintains the support of  $l_{CN}$  with a compressive force of  $k_2$ . Simultaneously,  $Q_2$  rotates around joint  $C$  as Hart's linkage operates. When the height displacement reached  $\Delta h_1$ , both  $Q_2$  and  $Q_3$  established contact with  $l_{CN}$  simultaneously. We define  $\Delta h_1$  as the compliance range. Subsequently,  $Q_2$  began pushing  $l_{CN}$  aside, thereby overcoming the compressive force of  $k_2$ . Hence,  $l_{CN}$  was detached from  $Q_3$  and tilted as its tip  $N$  shifted slightly on the surface. At the instant the height displacement reached  $\Delta h_2$ , joint  $D$  (which had a roller bearing in a prototype design, as will be discussed in Section V) established contact with the surface. In other words, the scooping pose was completed when both joint  $D$  and tip  $N$  established contact with the surface. We define  $\Delta h_2$  as the transition range. Therefore, the proposed finger undergoes a passive transition from the pinching pose to the scooping pose. The angle of  $Q_2$  was set as  $Q_2 = 47.68^\circ$ ; consequently, the compliance range  $\Delta h_1 = 30 \text{ mm}$  (or  $48 \text{ mm} \leq h \leq 78 \text{ mm}$ ) and the transition range  $\Delta h_2 = 10 \text{ mm}$  (or  $38 \text{ mm} \leq h < 48 \text{ mm}$ ), with an attack angle of  $\Delta\theta_{C1} = 22^\circ$  when the fingertip length was designed as  $l_{CN} = 27 \text{ mm}$ . All dimensions of the parallelogram and stoppers are listed in Table II.

#### IV. KINEMATICS AND STATICS

The kinematic models of the proposed finger are shown in Fig. 8. This model describes the fingertip sliding on an uphill surface and transitioning to the scooping pose, respectively. Based on the Plücker line coordinates presented in [32], the notations  $\hat{S}_i = \{y_i, -x_i; 1\} \in \mathbb{R}^3$  and  $\hat{S}'_i = \{\cos \theta_i, \sin \theta_i; 0\} \in \mathbb{R}^3$  denote the axis coordinates with respect to the rotor and slider of the  $i$ th joint in the plane, respectively.  $\hat{s}_{jk} = \{x_k - x_j, y_k - y_j; x_j y_k - y_j x_k\}/l_{jk} \in \mathbb{R}^3$  denotes the ray coordinates passing through both the  $j$ th and  $k$ th joints.

##### A. Fingertip Force Vector for Sliding on Uphill Surface

Referring to Fig. 8, the proposed finger was actuated along coordinates  $\hat{S}'_O$ , and then, the tip  $N$  slid on a surface along coordinates  $\hat{S}'_N$ . It was assumed that the fingertip  $l_{CN}$  was attached to the stopper  $Q_3$  during sliding on the surface with

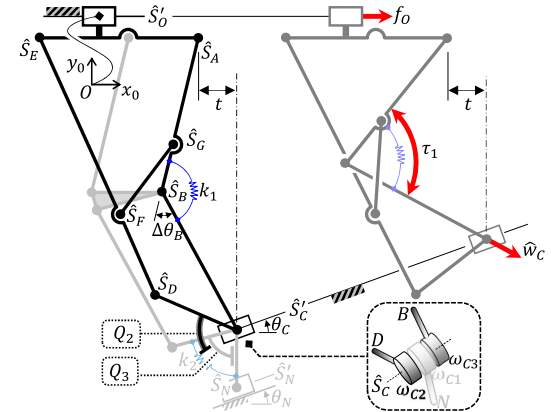


Fig. 8. Kinematic model of the proposed finger mechanism describing fingertip sliding on the uphill surface, satisfying  $\theta_C = \theta_N$ .

an acute angle of  $0^\circ \leq \theta_N < 90^\circ$ . Based on this assumption, the proximal tip  $C$  has the same movement as the distal tip  $N$ , i.e.,  $\theta_N = \theta_C$  (or  $\hat{S}'_N = \hat{S}'_C$ ) within the compliance range of  $48 \text{ mm} \leq h \leq 78 \text{ mm}$ . In other words, the tip  $N$  has the same force vector as tip  $C$ . Therefore, the kinematics need not be considered for the orientation of the fingertip.

Hart's linkage with a fingertip slider is composed of three kinematic chains,  $OABC$ ,  $OEDC$ , and  $AGFE$ . The first two chains are connected via the last one. Hence, the relationship between the input  $\nu_O$  and output  $\nu_C$ , the common variables of both  $OABC$  and  $OEDC$ , can be developed through the angular velocity relationship between  $\omega_A$  and  $\omega_E$  of  $AGFE$ .

First, the loop-closure equations of the chains  $OABC$  and  $OEDC$  are written as follows, respectively:

$$\nu_O \hat{S}'_O + \omega_A \hat{S}_A + \omega_B \hat{S}_B = \omega_{C3} \hat{S}_C + \nu_C \hat{S}'_C \quad (9)$$

$$\nu_O \hat{S}'_O + \omega_E \hat{S}_E + \omega_D \hat{S}_D = \omega_{C2} \hat{S}_C + \nu_C \hat{S}'_C \quad (10)$$

where  $\omega_n \in \mathfrak{R}$  for  $n = A, B, E, D, C_2, C_3$ , and  $\nu_m \in \mathfrak{R}$  for  $m = O, C$  denote the angular and linear velocities, respectively.  $\omega_A$  and  $\omega_E$  can be obtained in terms of the input and output velocities  $\nu_O$  and  $\nu_C$  by multiplying both sides of (9) and (10) with the ray coordinates  $\hat{s}_{BC}$  and  $\hat{s}_{CD}$  to form the reciprocal products to  $\hat{S}_B$ ,  $\hat{S}_C$ , and  $\hat{S}_D$ , respectively, as follows:

$$\omega_A = \nu_C \frac{\hat{s}_{BC}^T \hat{S}'_C}{\hat{s}_{BC}^T \hat{S}_A} - \nu_O \frac{\hat{s}_{BC}^T \hat{S}'_O}{\hat{s}_{BC}^T \hat{S}_A} \quad (11)$$

$$\omega_E = \nu_C \frac{\hat{s}_{DC}^T \hat{S}'_C}{\hat{s}_{DC}^T \hat{S}_E} - \nu_O \frac{\hat{s}_{DC}^T \hat{S}'_O}{\hat{s}_{DC}^T \hat{S}_E}. \quad (12)$$

Now, we need to obtain the relationship between  $\omega_A$  and  $\omega_E$  in the chain  $AGFE$ , and its loop-closure equation can be written as follows:

$$\omega_E \hat{S}_E = \omega_A \hat{S}_A + \omega_G \hat{S}_G + \omega_F \hat{S}_F. \quad (13)$$

Multiplying both sides of the aforementioned equation by ray coordinates  $\hat{s}_{FG}$  to form the reciprocal product,  $\omega_E$  can be

obtained in terms of  $\omega_A$  as

$$\omega_E = \omega_A \frac{\hat{s}_{FG}^T \hat{s}_A}{\hat{s}_{FG}^T \hat{s}_E}. \quad (14)$$

Substituting both (11) and (12) into the aforementioned equation yields the following input–output relationship:

$$\begin{aligned} \nu_O &= \nu_C \mathbf{U}^T \hat{s}_C, \text{ where } \mathbf{U} = \frac{\alpha \hat{s}_{CD} - \beta \hat{s}_{BC}}{\alpha \hat{s}_{CD}^T \hat{s}_O - \beta \hat{s}_{BC}^T \hat{s}_O} \in \mathbb{R}^3 \\ \alpha &= \hat{s}_{BC}^T \hat{s}_A \hat{s}_{FG}^T \hat{s}_E \in \mathbb{R}, \text{ and } \beta = \hat{s}_{FG}^T \hat{s}_A \hat{s}_{CD}^T \hat{s}_E \in \mathbb{R}. \end{aligned} \quad (15)$$

Next, the spring  $k_1$  installed in joint  $B$  of Hart's linkage can be considered as another input along with the actuating one of the base because the spring torque affects the output force as well. Hence, the relationship between the output linear velocity  $\nu_C$  and the input angular velocity  $\omega_B$ , which represents the instantaneous deformation of the spring, should be developed.  $\omega_B$  can be obtained multiplying both sides of (9) by ray coordinates  $\hat{s}_{AC}$  as follows:

$$\omega_B = \nu_C \frac{\hat{s}_{AC}^T \hat{s}'_C}{\hat{s}_{AC}^T \hat{s}_B} - \nu_O \frac{\hat{s}_{AC}^T \hat{s}'_O}{\hat{s}_{AC}^T \hat{s}_A}. \quad (16)$$

Substituting (15) into (16), we obtain

$$\omega_B = \nu_C \mathbf{V}^T \hat{s}_C, \text{ where } \mathbf{V} = \frac{\hat{s}_{AC} - (\hat{s}_{AC}^T \hat{s}'_O) \mathbf{U}}{\hat{s}_{AC}^T \hat{s}_B} \in \mathbb{R}^3. \quad (17)$$

Let  $f_O \in \mathbb{R}$  and  $\tau_{s1} \in \mathbb{R}$  be the actuation force at  $\hat{s}'_O$  and the spring torque at  $\hat{s}_B$ , respectively, as inputs. Subsequently, the instantaneous power is expressed as

$$\nu_O f_O + \omega_B \tau_{s1} = \nu_C \hat{w}_C^T \hat{s}'_C \quad (18)$$

where  $\hat{w}_C \in \mathbb{R}^3$  denotes the output wrench exerted by the proximal tip  $C$ . The spring torque can be defined as  $\tau_{s1} = -k_1 \Delta\theta_B$  where  $\theta_B$  denotes the relative angle of  $l_{BC}$  with respect to  $l_{AB}$ . Substituting both (15) and (17) into (18), we can obtain the statics equation that includes the spring effect, as follows:

$$\mathbf{G}^T \mathbf{f} = \hat{w}_C \quad (19)$$

where  $\mathbf{f} = [f_O \ \tau_{s1}]^T$  and  $\mathbf{G} = [\mathbf{U} \ \mathbf{V}] \in \mathbb{R}^{3 \times 2}$ . The first two rows of  $\hat{w}_C$  denote forces along the  $x$ - and  $y$ -axes, namely  $f_{Cx}$  and  $f_{Cy}$ , respectively. Recall that the distal tip  $N$  has the same force vector as the proximal tip  $C$ , i.e.,  $f_{Nx} = f_{Cx}$  and  $f_{Ny} = f_{Cy}$ . Hence, the force direction of tip  $N$  can be obtained using the inverse tangent function, i.e.,  $\theta_{Nf} = \text{atan2}(f_{Cy}, f_{Cx})$ .

Through the deviation between the fingertip force angle  $\theta_{Nf}$  and the surface angle  $\theta_N$ , whether the fingertip can slide can be indicated. For instance, let  $\theta_{Nn} = \theta_N - \pi/2$  be the normal angle of the surface for an intuitive comparison of these angles. A simulation for the fingertip sliding on a smooth uphill surface, as an example, was conducted as shown in Fig. 9. In this simulation, the stiffness coefficient of the spring and the input force were  $k_1 = 1 \text{ mNm/deg}$  and  $f_O = 10 \text{ N}$ , respectively. Owing to the significant deviation between  $\theta_{Nf}$  and  $\theta_{Nn}$ , the finger can easily adapt to the surface, satisfying  $\theta_{Nf} > \theta_{Nn}$ . However, when the fingertip was facing a steep ascent, satisfying  $\theta_{Nf} \leq \theta_{Nn}$ , it

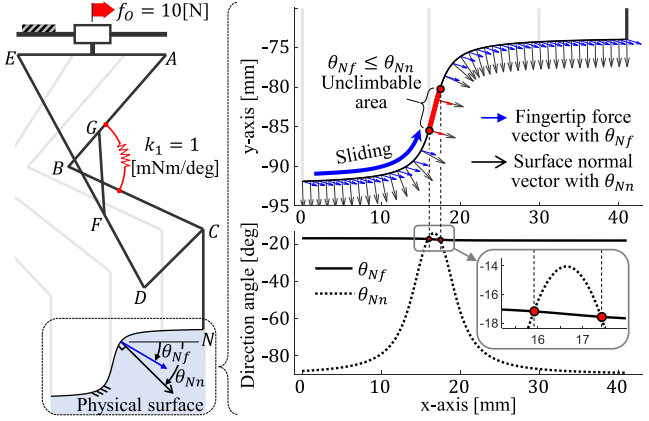


Fig. 9. Simulation of adapting to environment based on deviation of fingertip force angle and surface normal angle.

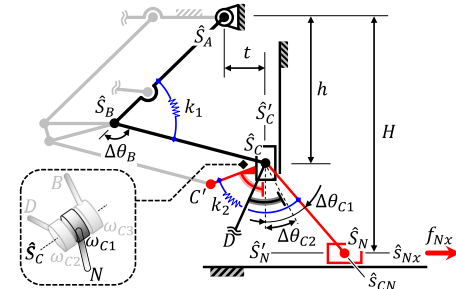


Fig. 10. Kinematic model of the proposed finger mechanism describing fingertip transitioning to scooping pose, configured as  $\theta_C = 90^\circ$  and  $\theta_N = 0^\circ$ .

could not slide on the ascent surface any longer because its sliding force (i.e., the pinching force projected onto the surface) was approximately zero. Therefore, the gripper should avoid facing extremely steep surfaces, or the manipulator should reposition the gripper with respect to such surfaces to satisfy  $\theta_{Nf} > \theta_{Nn}$ .

### B. Selection of Springs to Achieve Exact Scooping Pose

Referring to Fig. 7, the spring  $k_1$  consistently stored the elastic potential energy during finger flexion. After the stopper  $Q_2$  began pushing fingertip  $l_{CN}$  aside, the degree of the fingertip orientation was governed by the stiffness of the spring  $k_2$ . If this stiffness is extremely high, then a high pushing force of the manipulator is required to overcome the high spring torque  $\tau_{s2}$ . By contrast, if it is extremely low, then  $l_{CN}$  can easily drop to the surface as the energy of  $k_1$  is released. Hence, the appropriate stiffness should be selected for each spring such that the angular displacement of  $l_{CN}$  is aligned to that of  $Q_2$  with an appropriate pushing force of the manipulator, i.e.,  $\Delta\theta_{C1} = \Delta\theta_{C2}$ . This implies that the finger is in static equilibrium for every moment of the transition range, maintaining consistent contact between  $l_{CN}$  and  $Q_2$ . As shown in Fig. 10, an equivalent model of the finger mechanism describes the transition of the fingertip. With the linear actuation powered OFF, the proximal tip  $C$  can be expressed as the slider, which represents the vertical path instead of the transmission links ( $l_{CD}$ ,  $l_{DE}$ , and  $l_{FG}$ ), i.e.,  $\theta_C = 90^\circ$ . The distal tip  $N$  moves along the flat surface with  $\theta_N = 0^\circ$ ;

therefore,  $l_{CN}$  can be represented as a double-slider crank. By setting that  $\nu_O$  is equal to zero in (16),  $\omega_B$  denoting the instantaneous deformation of the spring  $k_1$  can be written in terms of  $\nu_C$  as follows:

$$\omega_B = \nu_C \frac{\hat{s}_{AC}^T \hat{S}'_C}{\hat{s}_{AC}^T \hat{S}_B} \quad (20)$$

which implies that an angular motion of the joint  $B$  generates a linear motion of the proximal tip  $C$ , describing a simple slider crank. And then, this motion of the tip  $C$  will generate another linear motion of the distal tip  $N$ , slipping on the surface. The kinematic chain  $CN$  including motions of two tips can be described as a double slider crank, and its loop-closure equation can be expressed as

$$\nu_C \hat{S}'_C + \omega_{C1} \hat{S}_C = \omega_N \hat{S}_N + \nu_N \hat{S}'_N. \quad (21)$$

$\nu_C$  and  $\omega_{C1}$  can be solved in terms of  $\nu_N$  by multiplying both sides of (21) with ray coordinates  $\hat{s}_{CN}$  and  $\hat{s}_{Nx}$  to form the reciprocal products, respectively, as follows:

$$\nu_C = \nu_N \frac{\hat{s}_{CN}^T \hat{S}'_N}{\hat{s}_{CN}^T \hat{S}'_C} \text{ and } \omega_{C1} = \nu_N \frac{\hat{s}_{Nx}^T \hat{S}'_N}{\hat{s}_{Nx}^T \hat{S}'_C} \quad (22)$$

where  $\hat{s}_{Nx} = \{1, 0; H\}$  denotes the lay coordinates parallel to the  $x$ -axis, including the position of the tip  $N$ .

Next, the instantaneous power with respect to the spring torques and the slipping force is expressed as

$$\omega_B \tau_{s1} + \omega_{C1} \tau_{s2} = \nu_N f_{Nx} \quad (23)$$

where  $f_{Nx}$  denotes the moving force of the tip  $N$  along  $\hat{s}_{Nx}$ . Similar to the aforementioned spring torque  $\tau_{s1}$ , the other spring torque is defined as  $\tau_{s2} = -k_2 \Delta \theta_{C1}$ . Substituting (20) and (22) into (23), yields

$$f_{Nx} = -k_1 \Delta \theta_B \frac{\hat{s}_{AC}^T \hat{S}'_C}{\hat{s}_{AC}^T \hat{S}_B} \frac{\hat{s}_{CN}^T \hat{S}'_N}{\hat{s}_{CN}^T \hat{S}'_C} - k_2 \Delta \theta_{C1} \frac{\hat{s}_{Nx}^T \hat{S}'_N}{\hat{s}_{Nx}^T \hat{S}'_C}. \quad (24)$$

Let  $\Delta \theta_{C1} = \Delta \theta_{C2}$  represent the consistent contact between  $Q_2$  and  $l_{CN}$ . Thereby, the total height  $H$  of  $\hat{s}_{Nx}$  corresponding to the  $y$ -axis position of the tip  $N$  can be kinematically defined as  $H = h + l_{CN} \cos \Delta \theta_{C2}$ . The static equilibrium of the springs depending on the height  $H$  can be solved when  $f_{Nx}$  in (24) is equal to zero, and then, the stiffness ratio of two springs can be obtained as follows:

$$\frac{k_2}{k_1} = -\frac{\Delta \theta_B}{\Delta \theta_{C2}} \frac{\hat{s}_{AC}^T \hat{S}'_C}{\hat{s}_{AC}^T \hat{S}_B} \frac{\hat{s}_{CN}^T \hat{S}'_N}{\hat{s}_{CN}^T \hat{S}'_C} \frac{\hat{s}_{Nx}^T \hat{S}'_N}{\hat{s}_{Nx}^T \hat{S}'_C}. \quad (25)$$

Fig. 11(a) shows the stiffness ratio of the two springs, where static equilibrium is reached based on the total height  $H$  within the transition range  $\Delta h_2$ . For the consistent contact of  $l_{CN}$  and  $Q_2$ , the maximum value of the ratio should be selected as  $k_2/k_1 = 1.5455$ . For instance, Fig. 11(b) shows the force  $f_{Nx}$  in (24) for all displacements of the finger when the stiffness was selected as  $k_1 = 1 \text{ mNm/deg}$ , and  $k_2 = 1.5455 \text{ mNm/deg}$ .  $f_{Nx}$  was equal to zero within the compliance range  $\Delta h_1$  since  $l_{CN}$  was parallel to the  $y$ -axis, which implies that the tip  $N$  is stationary on the surface. As soon as the displacement reached the transition range  $\Delta h_2$ , the tip  $N$  exerted a slipping force

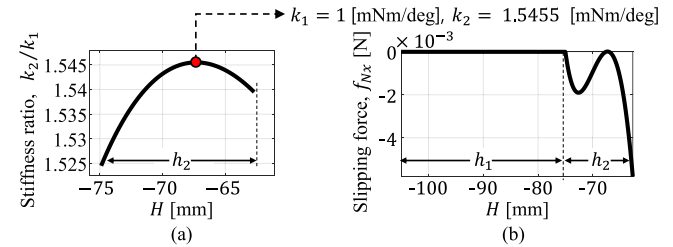


Fig. 11. Selection of spring stiffness.(a) Stiffness ratio satisfying static equilibrium according to the total height  $H$ . (b) Negative slipping force of  $f_{Nx}$  during transition to the scooping pose when  $k_2/k_1 = 1.5455$ .

with slightly negative magnitudes. This implies that the spring torque  $\tau_{S2}$  pushed  $Q_2$  against spring torque  $\tau_1$ . Consequently,  $Q_2$  and  $l_{CN}$  consistently exhibited the same angular displacement during the transition.

However, a prototype of the proposed finger was designed with springs of different types and stiffness coefficients to account for the space efficiency in the mechanical design as well as to enable the use of commercially available components. The spring torque  $\tau_1$  was designed by arranging two torsional springs with the same stiffness in parallel as total  $k_1 = 0.86 \text{ mNm/deg}$ , whereas the spring torque  $\tau_2$  was designed by arranging two linear springs with the same stiffness in parallel as total  $k_2 = 0.332 \text{ N/mm}$  between links  $l_{CC'}$  and  $l_{CN}$ . The stiffness of the linear springs was selected to have the joint torque aspect similar to the torsional spring with  $k_2 = 1.5455 \text{ mNm/deg}$  in Fig. 11(b) within the transition range.

## V. EXPERIMENTAL EVALUATION

In this section, we evaluate the human-inspired grasp capability shown in Fig. 1 for the proposed finger mechanism. A prototype was constructed, and several demonstrations were conducted. To prove the superiority of the prototype, small or thin objects that cannot be grasped by conventional grippers were used in the demonstrations.

### A. Prototype Design and Its Compliance Capability

The prototype was designed and installed on a classical parallel gripper of a commercial manipulator manufactured by Franka Emika GmbH as shown in Fig. 12. A pair of rigid jaws, which was the standard components of this parallel gripper, was replaced with a pair of prototypes via a mechanical adaptor that connects the prototype's base to the actuation component of the gripper (it is noteworthy that the prototype can be attached to other commercialized parallel gripper through a simple design modification of the mechanical adaptor). As shown in Fig. 12, a potentiometer to sense a joint angle was attached to the joint  $A'$  of the parallelogram, which had the same angle as joint  $A$  of Hart's linkage. Therefore, the height  $h$  based on the configuration of each finger can be calculated through kinematics. Moreover, an additional sharp tip fabricated using smooth plastic that can be customized based on the technical requirements of a particular task was attached to each fingertip to mitigate the impact between them and to allow the fingertip to easily slip

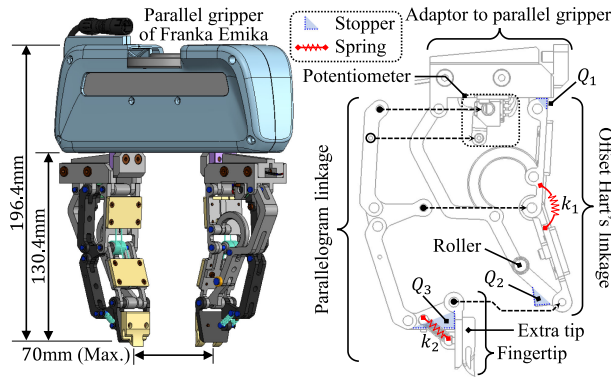


**Fig. 12.** Prototype design of the proposed finger mechanism on the parallel gripper of Franka Emika that is commercially available and its exploded view.

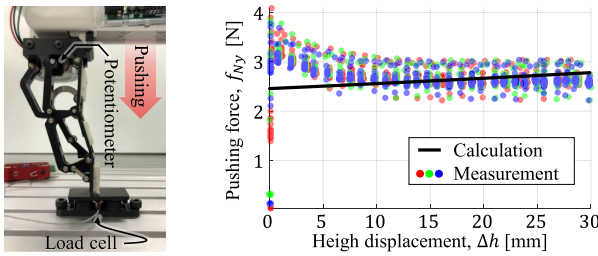


**Fig. 13.** Pushing force activated by deformation of the spring  $k_1$  based on height displacement  $\Delta h$ . Force and height were measured using load cell and potentiometer, respectively; experiment was conducted thrice.

under an object during scooping. As shown in Fig. 7, the joint  $D$  was in contact with the surface in the scooping pose. To reduce its sliding friction during scooping, a roller bearing was added to this joint.

The prototype was first tested for finger compliance. Fig. 13 shows the experimental setup and the measured results. While the manipulator vertically pushed the prototype in the compliance range  $\Delta h_1$ , a load cell and potentiometer simultaneously measured the pushing force and joint angle, respectively. The pushing of the manipulator created 1-s pauses at regular intervals of 1 mm. This experiment was conducted thrice (marked as red, green, and blue dots). The result shows that the peak of the measured force was approximately 4 N at the beginning of pushing; subsequently, the magnitudes gradually decreased to within 2.5–3 N, which is a force aspect similar to the calculation result. Therefore, the manipulator should have the capability of withstanding loads of these magnitudes during its interaction with the flat surface.

### B. Direct Pinching and Symmetric Scooping

Challenging tasks of grasping were performed with a pair of prototypes as shown in Fig. 14. As the manipulator intentionally pushed the gripper down, the fingertips established contact with the surface based on the vertical compliance. After the fingers completed touching down, the fingertips began to sweep on the surface through their closing motion. Subsequently, the gripper successfully pinched a microwrench tool and a thin plastic card



**Fig. 14.** Direct pinching microwrench and thin plastic card on the flat surface.

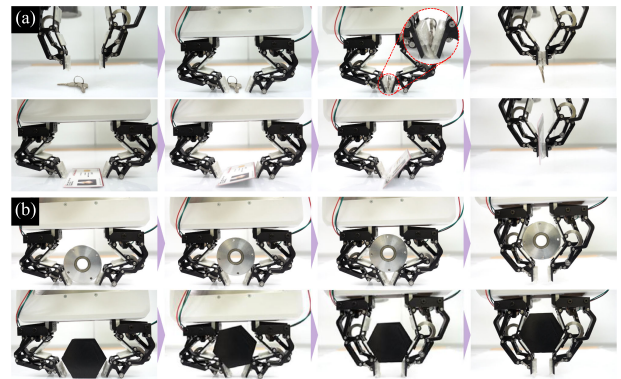


**Fig. 15.** Symmetric scooping. (a) Pinching a key and the thin plastic card. (b) Enveloping a cylindrical steel and hexagon object.

overhead despite the insufficient contact area of the side edges. However, when pinching the thin card, which had a relatively large width, the gripper could not fully constrain its instantaneous motion. Hence, the object was unstable during grasping.

To achieve a stable pinching grasp, a sufficient contact area between the thin object and fingertips should be ensured. Fig. 15 shows the symmetric scoop-and-pinch task of the gripper for grasping a key and a thin card. Each fingertip took the scooping pose at the height displacement of  $h = 38$  mm, contacting each roller with the flat surface. As shown at the top of Fig. 15(a), the key with a small width was cornered between the fingertips, which lifted slightly and rotated as soon as they slipped under the key. After the gripper departed from the contact surface, the key was stably pinched by the parallel fingertips. When scooping the thin card, one of the fingertips slipped under it, as shown at the bottom of Fig. 15(a). As the thin card rotated, the fingertips encountered a large contact area. As compared with the final configuration of directly pinching the same thin card in Fig. 14, we observed that the scooping allowed the object to be more stable.

In addition, the scooping pose guided the objects into an enveloping area. Fig. 15(b) shows the scoop-and-envelope task of the gripper for enveloping a cylindrical steel and hexagon object. During the closing motion, the fingertips guided the objects into the enveloping area. These objects were fully constrained by the first and second phalanges after the gripper departed from the contact surface. It is noteworthy that both the scoop-and-pinch and scoop-and-envelope tasks were performed in the same grasping process. Hence, whether the gripper pinched or enveloped an object from scooping was automatically determined by its shape and size.

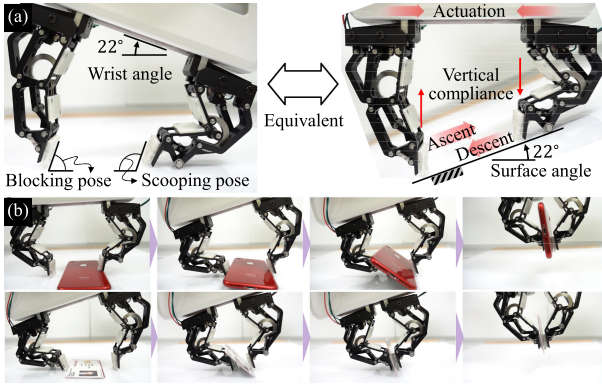


**Fig. 16.** Asymmetric scooping by the tilted wrist. (a) Equivalent representation of the wrist angle and surface angle. (b) Successful pinching grasp with steady object orientation via asymmetric scooping.

### C. Wrist Orientation for Asymmetric Scooping

As conducting the repetitive demonstrations depicted in Fig. 15(a), it was observed that the thin object rotated at different directions whenever scooping was performed, which was arbitrarily determined by one of the opposite fingertips early on. Moreover, both fingertips were simultaneously obstructed by the object's side edges, thereby preventing them from slipping under at times. To improve the scooping, the steady rotating direction of the object should be defined. Hence, the wrist orientation of the gripper based on the manipulator was considered in the scooping task. Fig. 16(a) shows the asymmetric configurations of the opposite fingers as the manipulator tilted the gripper. By pinning the fingertip of the fully stretched finger (left finger) to the flat surface, the parallel gripper rotated up to 22° in terms of the wrist angle. Simultaneously, the opposite finger (right finger) flexed until its roller established contact with the surface. Hence, each fingertip exhibited an acute angle pose and an obtuse angle pose from the gripper center where the objects were located. Therefore, it can be inferred that the former obstructed objects, whereas the latter slipped under them. In this section, the former and latter are called the blocking and scooping poses, respectively. The wrist orientation is analogous to considering a surface tilted at an angle of 22°. Hence, the blocking and scooping fingertips can be considered as facing an ascent and descent during the closing motion, respectively. Fig. 16(b) shows the asymmetric scoop-and-pinch task of the gripper, where the cellphone and thin plastic card rotated steadily. One side of the object was always rotated in the same scooping direction, whereas the blocking fingertip supported the other side. Therefore, the wrist orientation rendered the grasp more advantageous to pinching thin objects.

### D. Adaptive Pinching and Detection for Environments

Thus far, interactions with only a flat surface have been considered in grasping tasks. However, uneven environments exist in the real world. Based on the simulation shown in Fig. 9, we verified that the prototype can adapt to various environments. As demonstrated in Fig. 17, the gripper pulled off a small rectangular object in two environments. As shown in Fig. 17(a),

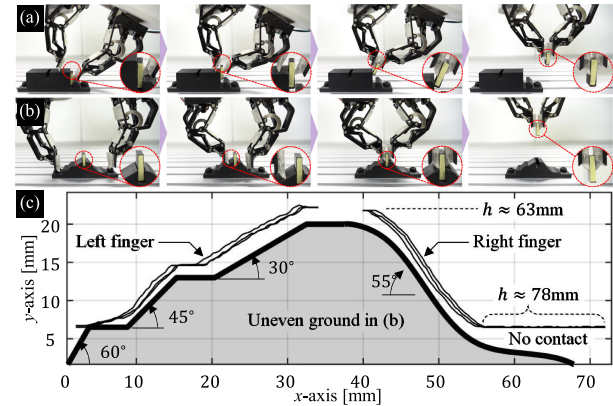


**Fig. 17.** Adaptation to environments. (a) Exploiting support of wall to pull out rectangular object in slot. (b) Sliding on uneven surface. (c) Locally detecting uneven surface using potentiometers.

the object was in a slot, in which one side was opened for the object. The gripper approached the object such that one fingertip established contact with one side via the open side of the slot. As the gripper activated the closing motion of the fingers, the force from the fingertip was applied to the object upward against the wall. Subsequently, the object began to ascend and slide along the wall. After the object reached the outer edge of the slot, the gripper successfully pinched it with robust adaptability to the environment.

Another challenging task was performed in a more uneven environment, as shown in Fig. 17(b) or (c). The ridge surfaces represent stairs and a smooth, wavy ascent. The climbing angles of the stairs were 60°, 45°, and 30° from bottom to top, whereas the maximal angle of the ascent was 55° in the middle. As shown in Fig. 17(b), the gripper successfully pinched the object slotted at the top, adapting to such an uneven environment. During this demonstration, the height  $h$  of each finger was calculated using the joint angle measured using the potentiometer while the gripper position was fixed. From the height calculations, the shape of the environment can be detected locally. Fig. 17(c) shows that the prototype can describe the shape of the environment similarly.

## VI. CONCLUSION

Herein, a fully passive finger mechanism that enables parallel grippers to interact with environmental constraints and human-inspired grasping motions to be implemented was proposed. The proposed finger mechanism featured two-DOF, i.e., the vertical translation and the orientation of the fingertip, constrained by springs and stoppers. These movements were driven only by interactions with constraints of objects or environments. Based on a case study pertaining to the interaction of fingers with environments, it was discovered that the finger compliance along the vertical translation perpendicular to the linear actuation of the base led to an effective interaction with environments. To mechanically embody the vertical compliance, Hart's linkage with the spring was introduced, and its linkage parameters were designed to exploit it as a finger mechanism, where an

initial posture was considered to immediately absorb the impact. Furthermore, the parallelogram linkage was employed to support the fingertip against reaction forces when pinching objects or sliding on surfaces, but allowing its orientation in the opposite direction for the scooping pose. Subsequently, Hart's linkage was coupled with the parallelogram linkage. To switch from the pinching pose to the scooping pose, the fingertip orientation was involved in the operation of Hart's linkage, where the range of the vertical translation was categorized into the compliance and transition ranges, defined as  $48 \text{ mm} \leq h \leq 78 \text{ mm}$  and  $38 \text{ mm} \leq h < 48 \text{ mm}$ , respectively. The functions of the proposed finger were investigated based on kinematics and statics, and several limitations were addressed. We noticed that the finger mechanism should avoid facing extremely steep surfaces because of the horizontal force direction of the fingertip. Moreover, this adaptation should be performed within the compliance range. Based on the static equilibrium for two springs within the transition range, the guideline for selecting the stiffness coefficient for each was presented such that the scooping pose of the fingertip would be well defined. Finally, the manufactured prototype of the proposed finger was installed to a parallel gripper to verify the feasibility and effectiveness of the finger compliance and grasping in environments, by performing several experiments and demonstrations. The results showed that the prototype can grasp objects such as a microwrench and a thin plastic card on a flat surface as well as can adapt to uneven environments. In particular, three grasping approaches inspired by human grasping motions, namely, adaptive pinching, symmetric scooping, and asymmetric scooping, were compared for their grasping qualities for the thin plastic card demonstration. It was discovered that asymmetric scooping rendered the thin object more stable in both the completion and grasping processes. Furthermore, the prototype demonstrated its ability in locally detecting the shape of an uneven environment using a potentiometer. This detectability is envisioned to benefit the visualization of local workspaces for performing robot manipulation and control. Further demonstrations concerning various objects are available in the attached supplementary video.

## REFERENCES

- [1] T. Laliberté, L. Birglen, and C. Gosselin, "Underactuation in robotic grasping hands," *Mach. Intell. Robot. Control*, vol. 4, no. 3, pp. 1–11, 2002.
- [2] M. B. Hong, S. J. Kim, Y. S. Ihn, G. Jeong, and K. Kim, "KULEX-hand: An underactuated wearable hand for grasping power assistance," *IEEE Trans. Robot.*, vol. 35, no. 2, pp. 420–432, Apr. 2019.
- [3] D. Yoon and Y. Choi, "Underactuated finger mechanism using contractible slider-cranks and stackable four-bar linkages," *IEEE/ASME Trans. Mechatronics*, vol. 22, no. 5, pp. 2046–2057, Oct. 2017.
- [4] M. H. Chang *et al.*, "Anthropomorphic prosthetic hand inspired by efficient swing mechanics for sports activities," *IEEE/ASME Trans. Mechatronics*, to be published, doi: [10.1109/TMECH.2021.3084311](https://doi.org/10.1109/TMECH.2021.3084311).
- [5] S. R. Kashef, S. Amini, and A. Akbarzadeh, "Robotic hand: A review on linkage-driven finger mechanisms of prosthetic hands and evaluation of the performance criteria," *Mech. Mach. Theory*, vol. 145, 2020, Art. no. 103677.
- [6] A. Chen, R. Yin, L. Cao, C. Yuan, H. K. Ding, and W. J. Zhang, "Soft robotics: Definition and research issues," in *Proc. IEEE Int. Conf. Mechatronics Mach. Vis. Pract.*, 2017, pp. 366–370.
- [7] R. Deimel and O. Brock, "A compliant hand based on a novel pneumatic actuator," in *Proc. IEEE Int. Conf. Robot. Autom.*, 2013, pp. 2047–2053.
- [8] R. Deimel and O. Brock, "A novel type of compliant and underactuated robotic hand for dexterous grasping," *Int. J. Robot. Res.*, vol. 35, no. 1–3, pp. 161–185, 2015.
- [9] C. Eppner, R. Deimel, J. Álvarez-Ruiz, M. Maertens, and O. Brock, "Exploitation of environmental constraints in human and robotic grasping," *Int. J. Robot. Res.*, vol. 34, no. 7, pp. 1021–1038, 2015.
- [10] M. G. Catalano, G. Grioli, E. Farnioli, A. Serio, C. Piazza, and A. Bicchi, "Adaptive synergies for the design and control of the Pisa/IIT SoftHand," *Int. J. Robot. Res.*, vol. 33, no. 5, pp. 768–782, 2014.
- [11] D. Mura, M. Barbarossa, G. Dinuzzi, G. Grioli, A. Caiti, and M. G. Catalano, "A soft modular end effector for underwater manipulation: A gentle, adaptable grasp for the ocean depths," *IEEE Robot. Automat. Mag.*, vol. 25, no. 4, pp. 45–56, Dec. 2018.
- [12] D. Yoon and Y. Choi, "Analysis of fingertip force vector for pinch-lifting gripper with robust adaptation to environments," *IEEE Trans. Robot.*, vol. 37, no. 4, pp. 1127–1143, Aug. 2021.
- [13] S. Aoyagi, M. Suzuki, T. Morita, T. Takahashi, and H. Takise, "Bellows suction cup equipped with force sensing ability by direct coating thin-film resistor for vacuum type robotic hand," *IEEE/ASME Trans. Mechatronics*, vol. 25, no. 5, pp. 2501–2512, Oct. 2017.
- [14] Z. Zhakypov, F. Heremans, A. Billard, and J. Paik, "An origami-inspired reconfigurable suction gripper for picking objects with variable shape and size," *IEEE Robot. Autom. Lett.*, vol. 3, no. 4, pp. 2894–2901, Oct. 2018.
- [15] Y. Hao *et al.*, "A multimodal, enveloping soft gripper: Shape conformation, bioinspired adhesion, and expansion-driven suction," *IEEE/ASME Trans. Robot.*, vol. 37, no. 2, pp. 350–362, Apr. 2020.
- [16] T. Ko, "A tendon-driven robot gripper with passively switchable underactuated surface and its physics simulation based parameter optimization," in *Proc. IEEE Int. Conf. Robot. Autom.*, 2020, vol. 5, no. 4, pp. 5002–5009.
- [17] K. Morino, S. Kikuchi, S. Chikagawa, M. Izumi, and T. Watanabe, "Sheet-based gripper featuring passive pull-in functionality for bin picking and for picking up thin flexible objects," *IEEE Robot. Autom. Lett.*, vol. 5, no. 2, pp. 2007–2014, Apr. 2020.
- [18] L. U. Odhner, R. R. Ma, and A. M. Dollar, "Precision grasping and manipulation of small objects from flat surfaces using underactuated fingers," in *Proc. IEEE Int. Conf. Robot. Autom.*, 2012, pp. 2830–2835.
- [19] L. U. Odhner, R. R. Ma, and A. M. Dollar, "Open-loop precision grasping with underactuated hands inspired by a human manipulation strategy," *IEEE Trans. Autom. Sci. Eng.*, vol. 10, no. 3, pp. 625–633, Jul. 2013.
- [20] L. U. Odhner *et al.*, "A compliant, underactuated hand for robust manipulation," *Int. J. Robot. Res.*, vol. 33, no. 5, pp. 736–752, 2014.
- [21] C. Jiang, A. Nazir, G. Abbasnejad, and J. Seo, "Dynamic flex-and-flip manipulation of deformable linear objects," in *Proc. IEEE/RSJ Int. Conf. Intell. Robots Syst.*, 2019, pp. 3158–3163.
- [22] V. Babin and C. Gosselin, "Picking, grasping, or scooping small objects lying on flat surfaces: A design approach," *Int. J. Robot. Res.*, vol. 37, no. 12, pp. 1484–1499, 2018.
- [23] V. Babin, D. St-Onge, and C. Gosselin, "Stable and repeatable grasping of flat objects on hard surfaces using passive and epicyclic mechanisms," *Robot. Comput. Integrat. Manuf.*, vol. 55, pp. 1–10, 2019.
- [24] T. Nishimura, K. Mizushima, Y. Suzuki, T. Tsuji, and T. Watanabe, "Variable-grasping-mode underactuated soft gripper with environmental contact-based operation," *IEEE Robot. Autom. Lett.*, vol. 2, no. 2, pp. 1164–1171, Apr. 2017.
- [25] F. Lévesque, B. Sauvet, P. Cardou, and C. Gosselin, "A model-based scooping grasp for the autonomous picking of unknown objects with a two-fingered gripper," *Robot. Auton. Syst.*, vol. 106, pp. 14–25, 2018.
- [26] T. He, S. Aslam, Z. Tong, and J. Seo, "Scooping manipulation via motion control with a two-fingered gripper and its application to bin picking," in *Proc. IEEE Int. Conf. Robot. Autom.*, 2021, vol. 6, no. 4, pp. 6394–6401.
- [27] W. J. Zhang and Y. Lin, "On the principle of design of resilient systems-application to enterprise information systems," *Enterprise Inf. Syst.*, vol. 4, no. 2, pp. 99–110, 2010.
- [28] H. Hart, "On some cases of parallel motion," in *Proc. London Math. Soc.*, vol. 8, no. 1, pp. 286–291, 1876.
- [29] L. Birglen, "Enhancing versatility and safety of industrial grippers with adaptive robotic fingers," in *Proc. IEEE/RSJ Int. Conf. Intell. Robots Syst.*, 2015, pp. 2911–2916.
- [30] L. Birglen, "Design of a partially-coupled self-adaptive robotic finger optimized for collaborative robots," *Auton. Robots*, vol. 43, no. 2, pp. 523–538, 2019.
- [31] H. Nolle, "Linkage coupler curve synthesis: A historical review-I. Developments up to 1875," *Mech. Mach. Theory*, vol. 9, no. 2, pp. 147–168, 1974.
- [32] J. Duffy, *Statics and Kinematics With Applications to Robotics*. New York, NY, USA:Cambridge Univ. Press, 1996.



**Dukchan Yoon** (Member, IEEE) received the B.S., M.S., and Ph.D. degrees in electronic systems engineering from Hanyang University (ERICA), Ansan, South Korea, in 2014, 2016, and 2020, respectively.

He is currently a Postdoctoral Researcher with the Department of Mechanical Engineering, Pohang University of Science and Technology, Pohang, South Korea. His research interests include the kinematic geometry, analysis, and synthesis of mechanisms based on the screw theory.



**Keehoon Kim** (Member, IEEE) received the B.S., M.S., and Ph.D. degrees in mechanical engineering from the Pohang University of Science and Technology, Pohang, South Korea, in 1999, 2001, and 2006, respectively.

He was a Visiting Student with the Case Western Reserve University, Cleveland, OH, USA, from 2003 to 2004. He was a Postdoctoral Researcher with the Department of Mechanical Engineering, Northwestern University, Evanston, IL, USA, from 2006 to 2009. He was

a Senior Research Scientist from 2009 to 2015 and a Principal Research Scientist from 2015 to 2019 with the Korea Institute of Science and Technology. From 2018 to 2019, he was a Visiting Professor with the Mechanical Engineering Department, University of Texas at Austin. He has been an Associate Professor with the Pohang University of Science and Technology since 2019. His research interests include robotics in biomedical applications, including rehabilitation robotics, surgical robotics, power assistant robotics and bionics, haptic interfaces, and teleoperation.

Dr. Kim served as an Editor for IEEE/RSJ International Conference on Intelligent Robots and Systems from 2015 to 2018. He has been serving as a Co-chair of the IEEE RAS Technical committee of Telerobotics since 2016.